



# Highly active TiO<sub>2</sub>/g-C<sub>3</sub>N<sub>4</sub>/G photocatalyst with extended spectral response towards selective reduction of nitrobenzene



Liqiang Zhang<sup>a,b,1</sup>, Xing He<sup>a,1</sup>, Xiuwen Xu<sup>a</sup>, Chao Liu<sup>a</sup>, Yongli Duan<sup>a</sup>, Liqiang Hou<sup>a</sup>, Qidong Zhou<sup>a,b</sup>, Chi Ma<sup>a,b</sup>, Xiaopeng Yang<sup>c</sup>, Rui Liu<sup>d</sup>, Fan Yang<sup>a</sup>, Lishan Cui<sup>a</sup>, Chunming Xu<sup>a</sup>, Yongfeng Li<sup>a,\*</sup>

<sup>a</sup> State Key Laboratory of Heavy Oil Processing, China University of Petroleum, Beijing 102249, China

<sup>b</sup> Department of Materials Science and Engineering, China University of Petroleum, Beijing 102249, China

<sup>c</sup> School of Materials Science and Engineering, University of Jinan, Jinan 250022, China

<sup>d</sup> State Key Laboratory of Environmental Chemistry and Ecotoxicology, Research Center for Eco-Environmental Sciences, Chinese Academy of Sciences, Beijing 100085, China

## ARTICLE INFO

### Article history:

Received 11 July 2016

Received in revised form 3 September 2016

Accepted 3 October 2016

Available online 4 October 2016

### Keywords:

TiO<sub>2</sub> nanowires

g-C<sub>3</sub>N<sub>4</sub> nanosheets

Graphene

Photocatalysis

## ABSTRACT

A simple self-assembly photochemical reduction method has been proposed to prepare highly photocatalytic TiO<sub>2</sub> nanowire/g-C<sub>3</sub>N<sub>4</sub> nanosheet/graphene heterostructures (TiO<sub>2</sub>/g-C<sub>3</sub>N<sub>4</sub>/G). In this hybrid structure, graphene enhances the charge transportation during photocatalytic process, and TiO<sub>2</sub> nanowires prevent graphene and g-C<sub>3</sub>N<sub>4</sub> from restacking. Meanwhile, g-C<sub>3</sub>N<sub>4</sub> with a more suitable band gap, extends the adsorption edge of the TiO<sub>2</sub>/g-C<sub>3</sub>N<sub>4</sub>/G composite to visual-region. Benefiting from the positive synergistic effect, 97% of nitrobenzene can be selectively reduced within 4 h by using TiO<sub>2</sub>/g-C<sub>3</sub>N<sub>4</sub>/G as the photocatalyst. The TiO<sub>2</sub>/g-C<sub>3</sub>N<sub>4</sub>/G composite with 3D structure demonstrates a great potential in selective oxidation and reduction of organics for the synthesis of high added-value organic compounds.

© 2016 Elsevier B.V. All rights reserved.

## 1. Introduction

Semiconductor based photocatalysis, a promising green chemical technique, is an approach to utilizing solar energy for hydrogen production [1], degradation of pollutions [2] and selective organic synthesis [3]. It is worth noting that the selective oxidation and reduction of organics for the synthesis of high added-value organic compounds have attracted much attention in recent years [4–6]. Aniline is one of the most important organic compounds and intermediates in the production of pharmaceuticals, food additives, agrochemicals, dye, and etc. [7,8]. In the past years, catalytic hydrogenation is a widely used for reducing nitrobenzene to aniline, which usually apply Pt, Pd, Au and transition metal as catalysts, NaBH<sub>4</sub> or H<sub>2</sub> reducing agents as additives. Additionally, this conversion process usually requires harsh reaction conditions, which greatly increases the product cost and fabrication difficult [8–11].

Recently, it is found that photocatalytic reduction technology demonstrates a great promising in the study of selective

organic synthesis. Being without involving of any environmentally unfriendly reducing agents and harsh reaction conditions, photocatalytic reduction is able to synthesize aniline in a green, low cost and effective way. As we known, titanium dioxide (TiO<sub>2</sub>) is a widely studied photocatalyst material possesses many advantages including high resistance to photocorrosion, chemical inertness, nontoxicity and low cost. However, the single TiO<sub>2</sub> semiconductor catalyst usually owns a poor activity, narrow spectral response and limited efficient electron transportation, which greatly degrades its performance. Recently, the fabrication of TiO<sub>2</sub> based composite materials is proved to be an effective strategy to improve its chemical activities [12–15]. In order to improve the poor charge transport property originated from TiO<sub>2</sub>, Zhang et al. incorporated TiO<sub>2</sub> with graphene for the first time in 2010 [16]. The results demonstrated that the trapping capability of graphene enhanced electron transportation and the as fabricated composite exhibited a high photocatalytic activity. Meanwhile, the easier organic molecule adsorption derived from the extended sp<sup>2</sup> hybrid carbon framework in graphene, along with its high UV light transparency, also contributed to the improvement of the photocatalytic activity [17–19]. Unfortunately, as TiO<sub>2</sub> nanoparticles own a large surface energy, they tend to aggregate during the reaction. Additionally, those TiO<sub>2</sub> in the form of nanoparticles cannot against the strong

\* Corresponding author at: College of Chemical Engineering, China University of Petroleum, 18# Fuxue Road, Changping, Beijing 102249, China.

E-mail addresses: [yfli@cup.edu.cn](mailto:yfli@cup.edu.cn), [liyongfeng2004@aliyun.com](mailto:liyongfeng2004@aliyun.com) (Y. Li).

<sup>1</sup> These authors contribute equally to this paper.

Van der Walls force between each graphene layer, which made them incapable of preventing graphene from restacking. In this context, efforts have been made to tailoring the morphology of TiO<sub>2</sub>, with a hope of resolving the aforementioned restacking and aggregation issues. Recently, one-dimensional TiO<sub>2</sub> nanostructures, including nanowires (NWs) [20,21], nanobelts [22–24] and so on, have triggered an explosion of research interests. For instance, Pan et al. [25] compared photocatalytic degradation performance between graphene/TiO<sub>2</sub> NWs and graphene/TiO<sub>2</sub> NPs composites and demonstrated that TiO<sub>2</sub> NWs, in comparison with TiO<sub>2</sub> NPs, had more uniform dispersion on graphene with less agglomeration. Also, the intercrossed TiO<sub>2</sub> NWs acted as the spacer between graphene nanosheets, which effectively prevented graphene from restacking, thereby endowing the composite catalyst with high stability and photocatalytic activity. More interestingly, as demonstrated by Sang et al. [22], in TiO<sub>2</sub> nanobelt/G composite, TiO<sub>2</sub> nanobelt with the unique 1D nanostructure can promote fast and efficient electron transport along the axial direction, which was conducive to the carrier separation during the photocatalytic process. It is therefore anticipated that the incorporation of graphene and 1D nanostructured TiO<sub>2</sub> would achieve dramatically enhanced charge transport properties associated with no obvious graphene restacking and TiO<sub>2</sub> agglomeration [26,27]. However, being limited by the narrow spectrum response stemmed from large band gap of TiO<sub>2</sub>, the performance of these 1D TiO<sub>2</sub>/graphene composite is still far from satisfactory.

In order to enhance the utilization of sunlight, namely extending the adsorption edge to visible light region, an effective strategy that incorporates TiO<sub>2</sub> based composite with other visible-light catalysts has been proposed. Visible-light catalysts previously investigated includes CdS [28], BiVO<sub>4</sub> [29], g-C<sub>3</sub>N<sub>4</sub> [30,31] etc. Among them, graphitic carbon nitride (g-C<sub>3</sub>N<sub>4</sub>), with a unique graphene-like 2D structure together with a band gap of about 2.7 eV, has attracted enormous attention as a photocatalyst. Similar to graphene, g-C<sub>3</sub>N<sub>4</sub> suffers from the inevitable restacking when being used alone. More seriously, it also possesses high recombination rate of photo-generated electron-hole pairs, which poses detrimental effect on its performance in photocatalysis. Thus, various strategies have been applied to overcome these shortcomings. For instance, Yang's group reported the synthesis of free-standing g-C<sub>3</sub>N<sub>4</sub> nanosheets by liquid phase exfoliation in isopropanol [32]. The ultrathin g-C<sub>3</sub>N<sub>4</sub> nanosheets, with large aspect ratios, high surface area and stoichiometric N/C ratio, exhibited good photocatalytic activity towards hydrogen evolution owing to the enhanced visible light absorption and improved photoluminescence quantum yield. Moreover, heterojunctions formed between different semiconductor materials, such as g-C<sub>3</sub>N<sub>4</sub>/Graphene [33], g-C<sub>3</sub>N<sub>4</sub>/CdS/G [34], Ag@AgVO<sub>3</sub>/G/PCN [35], can create great potential as the driving force to improve the separation of electron-hole pairs, which are proven to be effective photocatalysts to degrade organic pollutants under illumination.

Inspired by aforementioned insights, the TiO<sub>2</sub> NWs/g-C<sub>3</sub>N<sub>4</sub>/G nanocomposites were elaborately fabricated in this study. Specifically, graphene was introduced to enhance the charge transportation and separation during photocatalytic process. The incorporation of TiO<sub>2</sub> NWs were anticipated to show less agglomeration compared to that in nanoparticle form. Besides, they can act as skeleton between 2D nanosheet, thus preventing graphene and g-C<sub>3</sub>N<sub>4</sub> from restacking. More importantly, g-C<sub>3</sub>N<sub>4</sub> with a more suitable band gap extended the adsorption edge of the TiO<sub>2</sub> NWs/g-C<sub>3</sub>N<sub>4</sub>/G composite to visual-region, which significantly improved its photocatalytic performance towards selective reduction of nitrobenzene to aniline. It is found that the as fabricated TiO<sub>2</sub>/g-C<sub>3</sub>N<sub>4</sub>/G composites show significantly improved photocatalytic performance with a conversion of over 97% during a reaction

lasting for 4 h, exhibiting great potential in the field of selective photo reduction of organics.

## 2. Experimental

### 2.1. Synthesis of TiO<sub>2</sub> nanowires

TiO<sub>2</sub> NWs were synthesized by a hydrothermal method. Commercially available Degussa P25 was dissolved in 10 M NaOH solution and the concentration of P25 was 7.5 mg/mL. The homogeneous suspension was obtained by sonicating for 10 min and magnetically stirring for 30 min. Then the mixture was transferred to a Teflon vessel held in a stainless steel vessel at 180 °C for 12 h. Na<sub>2</sub>Ti<sub>8</sub>O<sub>17</sub> nanowire hydrogels were obtained and then ion exchanged into H<sub>2</sub>Ti<sub>8</sub>O<sub>17</sub> by acid treatment (0.2 M HNO<sub>3</sub>). After that, the hydrogen titanate nanowire materials were washed with excess deionized water until the filtrate became neutral and freeze-dried for further use. Finally, H<sub>2</sub>Ti<sub>8</sub>O<sub>17</sub> NWs were transformed into TiO<sub>2</sub> NWs by calcination at 600 °C for 4 h.

### 2.2. Synthesis of TiO<sub>2</sub>/g-C<sub>3</sub>N<sub>4</sub>/G nanocomposites

GO was prepared from natural graphite powder (Alfa Aesar, 325 mesh) by a modified Hummer's method [36]. Bulk g-C<sub>3</sub>N<sub>4</sub> was prepared by heating melamine from room temperature to 600 °C with a ramp rate of 2 °C/min and kept at this temperature for 4 h [1]. g-C<sub>3</sub>N<sub>4</sub> nanosheets were fabricated by one-pot exfoliation of bulk g-C<sub>3</sub>N<sub>4</sub> powder in isopropanol as solvent via a sonication. TiO<sub>2</sub>/g-C<sub>3</sub>N<sub>4</sub>/G heterojunctions were prepared via photochemical reduction self-assembly methods. Briefly, 20 mg GO was dispersed in 30 mL ethanol by ultrasonic to obtain Solution A. 150 mg g-C<sub>3</sub>N<sub>4</sub> nanosheets was dispersed in 50 mL ethanol by ultrasonic to make Solution B. 50 mg TiO<sub>2</sub> nanowires were dispersed in 30 mL ethanol under soft ultrasonication to obtain Solution C. Solutions A, B and C were mixed and stirred for 60 min. Then, the mixture was irradiated under 300 W xenon lamp for 4 h with stirring. The solution changed its color from brown to black, indicating that GO was reduced by the photocatalysts of g-C<sub>3</sub>N<sub>4</sub> and TiO<sub>2</sub> NWs and ethanol was the vacancy sacrificial reagent. The TiO<sub>2</sub>/g-C<sub>3</sub>N<sub>4</sub>/G heteroconjugates were obtained by washing with deionized water. The TiO<sub>2</sub>/g-C<sub>3</sub>N<sub>4</sub>/G powder was collected by vacuum drying for further experiments. For comparison, TiO<sub>2</sub>/G, g-C<sub>3</sub>N<sub>4</sub>/G were also prepared using similar methods without the presence of g-C<sub>3</sub>N<sub>4</sub> and TiO<sub>2</sub>, respectively.

### 2.3. Material characterization

The powder X-ray diffraction (XRD) measurements of as-prepared samples were recorded on the Bruker D8 Advance Germany using a graphite monochromator with Cu-K $\alpha$  radiation ( $\lambda = 1.5406 \text{ \AA}$ ). Raman spectra were recorded at room temperature using (InVia Reflex, Renishaw, UK) with a 532 nm laser excitation in the range of 800–3500 cm<sup>-1</sup>. X-ray photoelectron spectroscopy (XPS, Thermo Fisher K-Alpha American with an Al K $\alpha$  X-ray source) was used to measure the elemental composition of samples. The specific surface area was measured by using a nitrogen gas sorption surface area tester (JW-BK222, Beijing JWGB) and calculated by the Brunauer-Emmett-Teller (BET) method. The morphology of samples was characterized by FEI Quanta 200F scanning electron microscope (SEM) and the transmission electron microscope (TEM, Tecnai G2 F20) equipped with selected area electron diffraction (SAED). A drop of the g-C<sub>3</sub>N<sub>4</sub> supernatant was deposited on a mica substrate for atomic force microscope (AFM) observation (Bruker, Multimode 8). Thermal gravimetric analysis (TGA) was conducted in oxygen at a heating rate of 10 °C/min. The diffuse reflectance absorption spectra (DRS) of the samples were recorded

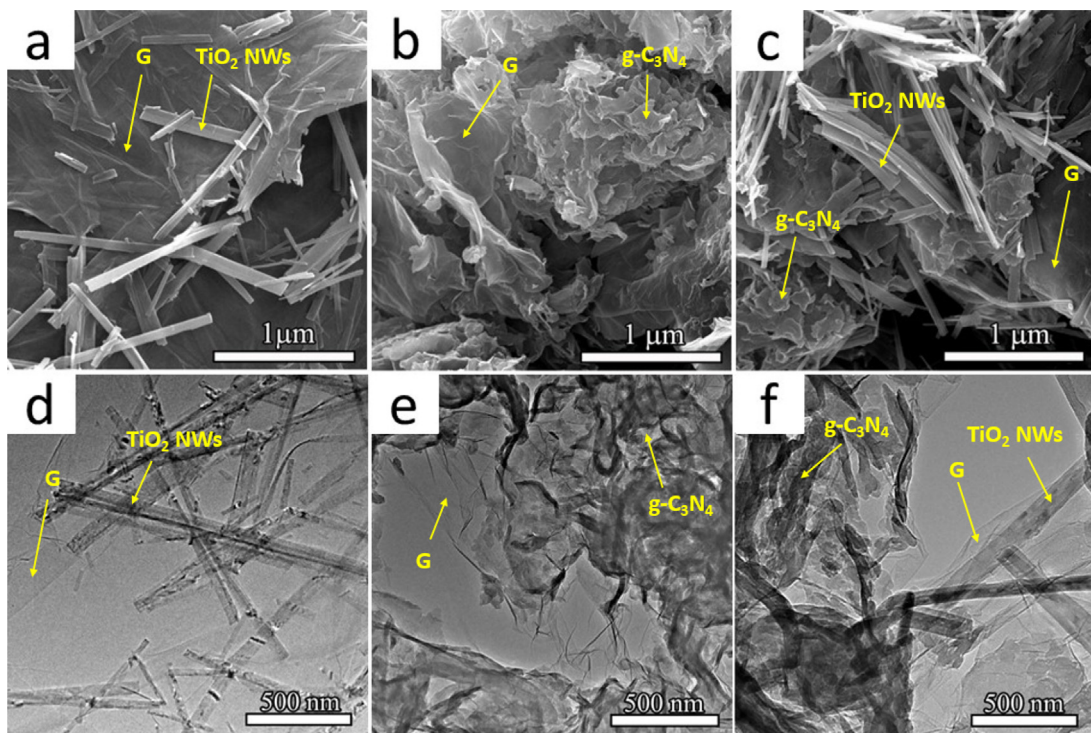


**Fig. 1.** SEM images of (a)  $\text{TiO}_2/\text{G}$ , (b)  $\text{g-C}_3\text{N}_4/\text{G}$  and (c)  $\text{TiO}_2/\text{g-C}_3\text{N}_4/\text{G}$ ; TEM images of (d)  $\text{TiO}_2/\text{G}$ , (e)  $\text{g-C}_3\text{N}_4/\text{G}$  and (f)  $\text{TiO}_2/\text{g-C}_3\text{N}_4/\text{G}$ .

by a UV-vis spectrophotometer in the range from 200–800 nm equipped with an integrated sphere attachment and  $\text{BaSO}_4$  as a reference standard. PL emission spectra were characterized at room temperature with a luminescence spectrophotometer (FLSP920, Edinburgh Instruments) using a Xenon laser with a 312 nm excitation light. The photocurrents were detected by using a standard three-electrode cell with  $\text{Ag}/\text{AgCl}$  as reference electrode and Pt wire as the counter electrode in KCl solution (3 M). Electrochemical impedance spectroscopy (EIS) and Cyclic voltammograms (CV) measurements were obtained using an electrochemical workstation (Corrtest Corporation, Wuhan, China).

#### 2.4. Photocatalytic reduction of nitrobenzene

Experiments were carried out in an apparatus specially designed for the photocatalytic reaction. For each photocatalytic reaction, 100 mg of the photocatalyst was dispersed in 50 mL of NB (nitrobenzene) in methanol solution (10 mM) by ultrasonication. The resultant mixture solution was then subjected to ultrasonic dispersion and stirring in dark for 30 min. Successively,  $\text{N}_2$  was introduced for 30 min before illumination in order to remove the dissolved oxygen. After the absorption-desorption equilibrium was achieved, the photocatalytic reaction was initiated by illumination with  $\text{N}_2$  atmosphere maintained. At certain intervals of time, aliquots (3 mL) of the solution were taken out. After being centrifuged to remove the photocatalysts, The NB and the resulting photocatalytic products were analyzed by an Agilent Technolgyies 7890AGC system. The chromate graphic conditions applied for photocatalytic reduction of nitrobenzene are summarized in Table S1. The conversion of nitrobenzene, yield of aniline and selectivity of aniline were calculated according to the following equations:

$$\text{Conversion}(\%) = [(C_0 - C_{NB})/C_0] \times 100$$

$$\text{Yield}(\%) = C_{\text{aniline}}/C_0 \times 100$$

$$\text{Selectivity}(\%) = [C_{\text{aniline}}/(C_0 - C_{NB})] \times 100$$

where  $C_0$  is the whole amount of NB in the solution before illumination;  $C_{NB}$  is the amount of NB in the solution after illumination for 4 h;  $C_{\text{aniline}}$  is the amount of aniline in the solution after illumination for 4 h.

## 3. Results and discussion

### 3.1. SEM and TEM

The SEM and TEM images of GO,  $\text{g-C}_3\text{N}_4$ ,  $\text{TiO}_2$  NWs and their composites were shown in Figs. 1 and S1, respectively. It is clearly observed that GO consists of continuous, thin and wrinkle-enriched graphene nanosheets (Fig. S1a and d),  $\text{g-C}_3\text{N}_4$  exhibits a two-dimensional (2D) structure with rugged surface (Fig. S1b and e), and  $\text{TiO}_2$  NWs were one-dimensional (1D) wires with diameters around hundred nanometers and length up to  $\mu\text{m}$ -scale (Fig. S1c and f). According to AFM image (Fig. S2), the thickness of exfoliated  $\text{g-C}_3\text{N}_4$  nanosheets is around 4.3 nm. In order to improve the poor charge transport,  $\text{TiO}_2$  NWs were rationally incorporated with graphene, as illustrated in Fig. 1a and d. Interestingly, in the  $\text{TiO}_2/\text{G}$  composite,  $\text{TiO}_2$  NWs, with flawless linear structure and no aggregation, are well dispersed with graphene nanosheets, thus  $\text{TiO}_2$  NW can act as skeleton between graphene nanosheets. Composite with such a structure is expected to show no graphene restacking and  $\text{TiO}_2$  aggregation, which is conducive to its stability during photocatalytic process. The SEM and TEM images of  $\text{g-C}_3\text{N}_4/\text{G}$  illustrated in Fig. 1b and e show that the  $\text{C}_3\text{N}_4$  with uneven surface are uniformly dispersed in wrinkle-enriched graphene. What's more, aiming to broaden the light response to visible region,  $\text{g-C}_3\text{N}_4$ , with a desired band gap of 2.70 eV, was further introduced, thus forming a  $\text{TiO}_2/\text{g-C}_3\text{N}_4/\text{G}$  composite, as shown in Figs. 1c and f and S1g and h. After incorporate  $\text{TiO}_2/\text{g-C}_3\text{N}_4/\text{G}$  (Fig. 1c and f), it is shown that  $\text{TiO}_2$  NWs are interpenetrated among graphene and  $\text{C}_3\text{N}_4$  layers successfully with no aggregation. So far, it can be concluded that a new kind of material with good morphology has been incorporated. Because of the excellent morphology, the new material

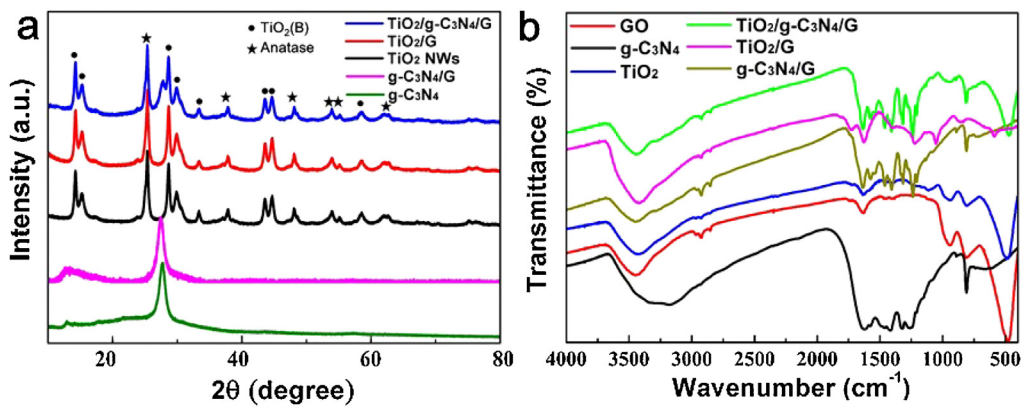


**Fig. 2.** (a) XRD patterns of TiO<sub>2</sub> NWs, g-C<sub>3</sub>N<sub>4</sub>, TiO<sub>2</sub>/G, g-C<sub>3</sub>N<sub>4</sub>/G, and TiO<sub>2</sub>/g-C<sub>3</sub>N<sub>4</sub>/G; (b) FTIR spectra of GO, TiO<sub>2</sub> NWs, g-C<sub>3</sub>N<sub>4</sub>, g-C<sub>3</sub>N<sub>4</sub>/G, TiO<sub>2</sub>/G and TiO<sub>2</sub>/g-C<sub>3</sub>N<sub>4</sub>/G.

probably reveals that respective advantages might be expressed, such as graphene is able to enhance the electron transfer properties, C<sub>3</sub>N<sub>4</sub> can increase the visible light response. Thus, further characterizations have been done as the following.

### 3.2. XRD and FTIR characterization

Fig. 2a shows the XRD patterns of the synthesized photocatalysts, which provide more information on their specific crystal structures. It is found that there are noticeable diffraction peaks appearing for TiO<sub>2</sub> NWs, and according to the standard PDF card, all these peaks can be ascribed to either anatase TiO<sub>2</sub> or TiO<sub>2</sub> (B) [22,37], which are marked as dots and stars, respectively. Interestingly, after introducing graphene, the TiO<sub>2</sub>/G shows almost the same XRD patterns compared to that of TiO<sub>2</sub> NWs, indicating the negligible effect graphene poses upon the TiO<sub>2</sub> NWs crystal structure. As validated by SEM and TEM, graphene does exist in the composites, while the absence of the characteristic peak of graphene is probably as a result of the highly dispersed graphene without any restacking and the relatively low content of graphene in the composite [38,39]. Moreover, in the case of TiO<sub>2</sub>/g-C<sub>3</sub>N<sub>4</sub>/G, an additional peak observed at 27.3° is characteristic interlayer stacking reflection of conjugated aromatic systems, indexed for graphitic materials as the (002) peak, suggesting the successful incorporation of g-C<sub>3</sub>N<sub>4</sub>. Moreover, the characteristic peak at 13.1° indexed to (100) crystal plane with a much weaker intensity clearly agree with other published reports [32,40], demonstrating that the layered g-C<sub>3</sub>N<sub>4</sub> has been successfully exfoliated as we expected.

For further investigation on their chemical compositions, FT-IR spectra of the as fabricated photocatalysts were characterized, as shown in Fig. 2b. In the spectrum of GO, prominent adsorption peaks are observed at 3420, 1732, 1620, 1401, 1226 and 1050 cm<sup>-1</sup>, which correspond to the stretching vibrations of O—H, C=O, aromatic C=C, carboxyl C—O, epoxy C—O and alkoxy C—O, respectively [41]. Evidently, the aforementioned absorption peaks of oxygen-containing functional groups decrease after GO incorporated into composites, due to the photocatalytic reduction of GO. In the case of pure g-C<sub>3</sub>N<sub>4</sub>, the characteristic peaks at 1640 cm<sup>-1</sup>, 1247 cm<sup>-1</sup>, 1325 cm<sup>-1</sup> and 1408 cm<sup>-1</sup> are clearly identified, which are induced by the stretching vibration of CN heterocycles, while the additional peaks at 808 cm<sup>-1</sup> and 3150~3500 cm<sup>-1</sup> can be attributed to a typical 3-s-triazine ring vibration and the stretching vibration of N—H and —OH, respectively [35,42]. Moreover, the characteristic absorption peaks of TiO<sub>2</sub> NWs were detected in the wavelength range of 500~700 cm<sup>-1</sup> [43]. It is obviously illustrated that the spectra of all composites are in high agreement with their corresponding components, demonstrating the successful fabrication of the target composites.

### 3.3. XPS analysis

XPS was performed to monitor the chemical composition and binding configurations of the photocatalysts. The XPS survey spectrum of TiO<sub>2</sub>/g-C<sub>3</sub>N<sub>4</sub>/G in Fig. 3a indicates the existence of C, N, O and Ti element, with their corresponding atomic proportions of 47.99%, 9.56%, 30.55% and 11.90%, respectively. Compared to the high resolution C 1s peak of GO in Fig. 3b, C 1s peak of TiO<sub>2</sub>/g-C<sub>3</sub>N<sub>4</sub>/G (Fig. 3c) shows no peaks that can be ascribed to C—O and O=C=O binding configurations, with a minor peak indexed to C=O, suggesting the removal of oxygen-containing functional groups because of the photocatalytic reduction of GO [35,41]. Besides, the additional peak appearing at 288.3 eV in C 1s peak attributes to C-(N)<sub>3</sub>, which is consistent with the dominating N-(C)<sub>3</sub> binding configuration detected in N 1s peak (Fig. 3d), demonstrating the successful incorporation of g-C<sub>3</sub>N<sub>4</sub>. The high resolution N 1s spectrum of TiO<sub>2</sub>/g-C<sub>3</sub>N<sub>4</sub>/G can be separated into two peaks. The dominant peak is ascribed to the sp<sup>2</sup> bonded nitrogen in thiazine rings [44], and the little peak at 401.1 eV is attributed to the bridging N atom N(C)<sub>3</sub> or N bonded with H atoms [35]. Moreover, the high resolution Ti 2p spectrum of XPS in Fig. S3a reveals that two peaks at ~459.1 and ~464.7 eV correspond to Ti 2p<sub>3/2</sub> and Ti 2p<sub>1/2</sub>, respectively, and according to the O 1s peak presented in Fig. S3, Ti—O peak at 530.5 eV accounts for 76.9% of the O bearing group, which further confirms the reduction of GO and the existence of TiO<sub>2</sub>. According to the TG results shown in Fig. S4, the specific contents of TiO<sub>2</sub>/G and TiO<sub>2</sub>/g-C<sub>3</sub>N<sub>4</sub>/G are determined to be 81.4 wt% and 54.9 wt%, respectively.

### 3.4. Raman and UV-vis characterization

Raman spectroscopy is also one of the most sensitive and informative techniques to characterize disorders in sp<sup>2</sup> carbon materials. The Raman spectra for GO, TiO<sub>2</sub>/G, g-C<sub>3</sub>N<sub>4</sub>/G and TiO<sub>2</sub> g-C<sub>3</sub>N<sub>4</sub>/G samples are shown in Fig. 4b respectively. The prominent bands located at 1350 and 1588 cm<sup>-1</sup> correspond to the D and G bands of the GO sample, where the D band is assigned to the defects and disordered atomic arrangements of sp<sup>3</sup> hybridized carbon atoms and the G band is a result of the plane vibration of sp<sup>2</sup> hybridized carbon atoms of the 2D GO layer [45]. The ratio of D/G band intensity ( $I_D/I_G$ ) of GO is calculated to be 0.95, while that of the TiO<sub>2</sub>/G, g-C<sub>3</sub>N<sub>4</sub>/G, TiO<sub>2</sub> and g-C<sub>3</sub>N<sub>4</sub>/G are 0.97, 0.95 and 0.99, respectively. Upon the photocatalytic reduction of GO,  $I_D/I_G$  is slightly increased, which can be explained by the formation of more sp<sup>2</sup> domains but with smaller domain sizes thus producing more boundaries within graphene framework [46]. Additionally, the N<sub>2</sub> adsorption-desorption isotherms shown in Fig. S5 exhibits a type IV curve with a distinct H3-type hystere-

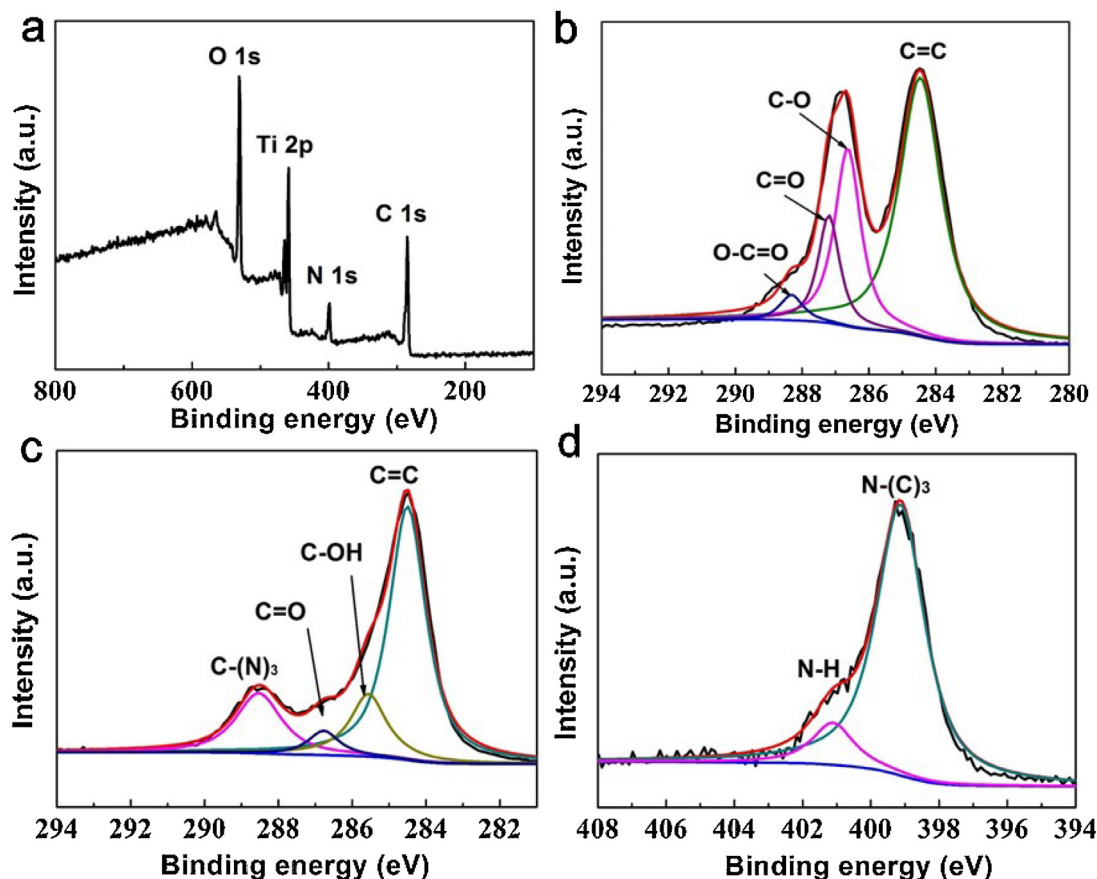


**Fig. 3.** (a) XPS spectrum of  $\text{TiO}_2/\text{g-C}_3\text{N}_4/\text{G}$ ; (b) C 1s XPS spectrum of GO; (c) C 1s and (d) N 1s XPS spectra of  $\text{TiO}_2/\text{g-C}_3\text{N}_4/\text{G}$ .

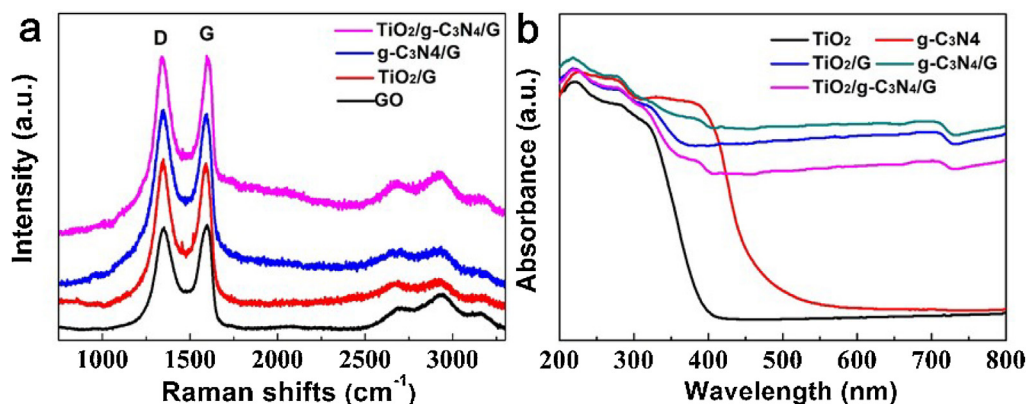


**Fig. 4.** (a) Raman spectra of GO,  $\text{TiO}_2/\text{G}$ ,  $\text{g-C}_3\text{N}_4/\text{G}$  and  $\text{TiO}_2/\text{g-C}_3\text{N}_4/\text{G}$ ; (b) UV-vis diffuse reflection of the as-synthesized  $\text{TiO}_2$  NWs,  $\text{g-C}_3\text{N}_4$ ,  $\text{TiO}_2/\text{G}$ ,  $\text{g-C}_3\text{N}_4/\text{G}$  and  $\text{TiO}_2/\text{g-C}_3\text{N}_4/\text{G}$ .

sis loop at relative pressure of 0.7–1.0, indicating the existence of macropores, and the detailed results are summarized in Table S1. Among all the photocatalysts prepared,  $\text{TiO}_2/\text{g-C}_3\text{N}_4/\text{G}$  exhibits a comparatively high SSA of  $90.63 \text{ m}^2 \text{ g}^{-1}$ . The relatively larger SSA of  $\text{TiO}_2/\text{g-C}_3\text{N}_4/\text{G}$  nanocomposites is probably as a result of the less aggregated 2D graphic materials with the bridging 1D  $\text{TiO}_2$  NWs acting as a spacer between 2D nanosheets (G and  $\text{g-C}_3\text{N}_4$ ).

To investigate the light absorption response of the as prepared catalyst, UV-vis diffuse reflection spectra were recorded, as shown in Fig. 4b. The pristine  $\text{TiO}_2$  NWs show the fundamental absorption edge rising at 390 nm, which agrees well with the intrinsic band gap

of 3.2 eV. As for  $\text{g-C}_3\text{N}_4$ , the absorption edge is extended to nearly 500 nm, as a result of its relatively narrow band gap. After the incorporation of graphene, the composites show light response towards visible light due to the presence of black graphene. Therefore, we can conclude that  $\text{g-C}_3\text{N}_4$  has noticeable response towards visible light, and the introduction of graphene significantly enhances the light absorption, thus rendering the composites with great potential as high catalytic activities over full spectrum light. In addition, the accurate band gap of the  $\text{TiO}_2$  NWs and  $\text{g-C}_3\text{N}_4$  can be calculated from the corresponding UV-vis diffuse reflection spectra, as shown in Fig. S6. It can be clearly seen that the band gaps of  $\text{TiO}_2$  NWs and  $\text{g-C}_3\text{N}_4$  are found to be 3.24 eV and 2.71 eV, respectively.

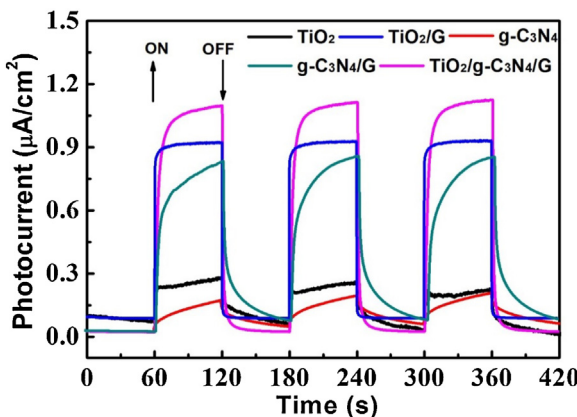


**Fig. 5.** Photocurrent response of the photo anodes of  $\text{TiO}_2$  NWs,  $\text{g-C}_3\text{N}_4$ ,  $\text{TiO}_2/\text{G}$ ,  $\text{g-C}_3\text{N}_4/\text{G}$  and  $\text{TiO}_2/\text{g-C}_3\text{N}_4/\text{G}$  samples.

### 3.5. Photocurrent response and EIS

To clarify the enhancement of graphene and  $\text{g-C}_3\text{N}_4$  upon the photocatalytic properties of the  $\text{TiO}_2/\text{g-C}_3\text{N}_4/\text{G}$  composite, the photo-electrochemical (PEC) performances of all the photocatalysts were systematically compared, as shown in Fig. 5. Owing to the outstanding charge-transport property of graphene [47], the  $\text{TiO}_2/\text{G}$  exhibits considerably increased constant photocurrent ( $0.90 \mu\text{A}/\text{cm}^2$ ), which is 3 times of that for  $\text{TiO}_2$  NWs ( $0.30 \mu\text{A}/\text{cm}^2$ ), and the  $\text{g-C}_3\text{N}_4/\text{G}$  also experiences a similar enhancement in photocurrent relative to that of pure  $\text{g-C}_3\text{N}_4$ . It is worthy to mention that compared to pure  $\text{TiO}_2$  NWs, the delay in the photocurrent of  $\text{TiO}_2/\text{G}$  has been noticeably eliminated. Unfortunately, the improvement of the delay effect with respect to  $\text{g-C}_3\text{N}_4/\text{G}$  is far from satisfactory, which might be resulted from the extremely poor electrical conductivity of  $\text{g-C}_3\text{N}_4$  and rather limited layer-to-layer contact between 2D  $\text{g-C}_3\text{N}_4$  and G nanosheets. Obviously, the as fabricated  $\text{TiO}_2/\text{g-C}_3\text{N}_4/\text{G}$  composite yields the highest photocurrent of  $1.1 \mu\text{A}/\text{cm}^2$ , indicating more electrons have been generated and transferred. It is assumed that the incorporation of  $\text{g-C}_3\text{N}_4$  renders the composite with an enhanced capacity towards light adsorption, and the existence of graphene facilitates the electron-hole separation and transportation during photocatalytic process [35,48], which endows the  $\text{TiO}_2/\text{g-C}_3\text{N}_4/\text{G}$  with great potential to be a highly active photocatalyst.

EIS was further conducted to investigate the transfer and separation efficiency of photogenerated charges using various photocatalysts, and the as obtained Nyquist diagram is depicted in Fig. 6. Generally, each arc in the diagram represents a resistance

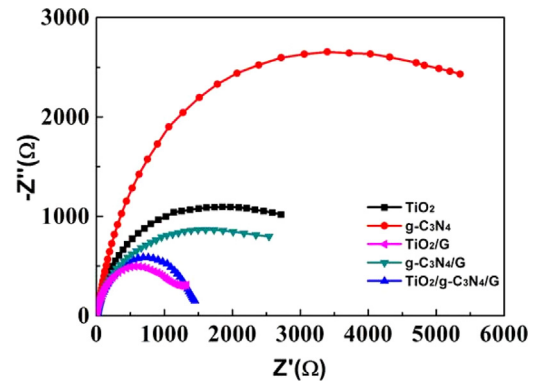


**Fig. 6.** EIS curves of as prepared  $\text{TiO}_2$  NWs,  $\text{g-C}_3\text{N}_4$ ,  $\text{TiO}_2/\text{G}$ ,  $\text{g-C}_3\text{N}_4/\text{G}$  and  $\text{TiO}_2/\text{g-C}_3\text{N}_4/\text{G}$  samples.

during the charge transfer process, and a smaller radius correlates to a lower charge-transfer resistance. Accordingly, it is evident that compared to other photocatalysts,  $\text{TiO}_2/\text{G}$  and  $\text{TiO}_2/\text{g-C}_3\text{N}_4/\text{G}$  composites show much smaller charge transfer resistance, although the introduction of  $\text{g-C}_3\text{N}_4$  leads to a negligible increase in the charge-transfer resistance [35]. However, by virtue of the effective adsorption of  $\text{g-C}_3\text{N}_4$  towards light with wavelength ranging from 390 nm to 500 nm, it is anticipated that the disadvantage caused by the incorporation of  $\text{g-C}_3\text{N}_4$  can be offset to some extent. Therefore, it is reasonable to conclude that the findings in EIS agree well with the results obtained by UV-vis and photoresponse measurements.

### 3.6. Photocatalytic properties of $\text{TiO}_2/\text{g-C}_3\text{N}_4/\text{G}$

In order to evaluate the photocatalytic activities of the as-prepared photocatalysts, the selective photocatalytic reduction of nitrobenzene to aniline was conducted in a photochemical reactor. The photocatalytic performances of  $\text{TiO}_2$  NWs,  $\text{g-C}_3\text{N}_4$ ,  $\text{TiO}_2/\text{G}$ ,  $\text{g-C}_3\text{N}_4/\text{G}$  and  $\text{TiO}_2/\text{g-C}_3\text{N}_4/\text{G}$  photocatalysts are illustrated in Fig. 7. As expected, the total conversion of nitrobenzene using pure  $\text{TiO}_2$  and  $\text{g-C}_3\text{N}_4$  as the photocatalyst merely reach 34.1% and 26.1%. In the case of  $\text{TiO}_2/\text{G}$  and  $\text{g-C}_3\text{N}_4/\text{G}$ , it is significantly increased to 72.0% and 64.8%, respectively, indicating that the high electron mobility and easier organic molecule adsorption derived from the extended  $\text{sp}^2$  hybrid carbon framework in graphene, along with its high UV light transparency, contribute to the improvement of the photocatalytic activity [48,49]. Benefiting from the positive synergistic effect of the three components, the  $\text{TiO}_2/\text{g-C}_3\text{N}_4/\text{G}$  composite exhibits a highest conversion efficiency of 97%, which means that almost all of the nitrobenzene can be converted within 4 h. The

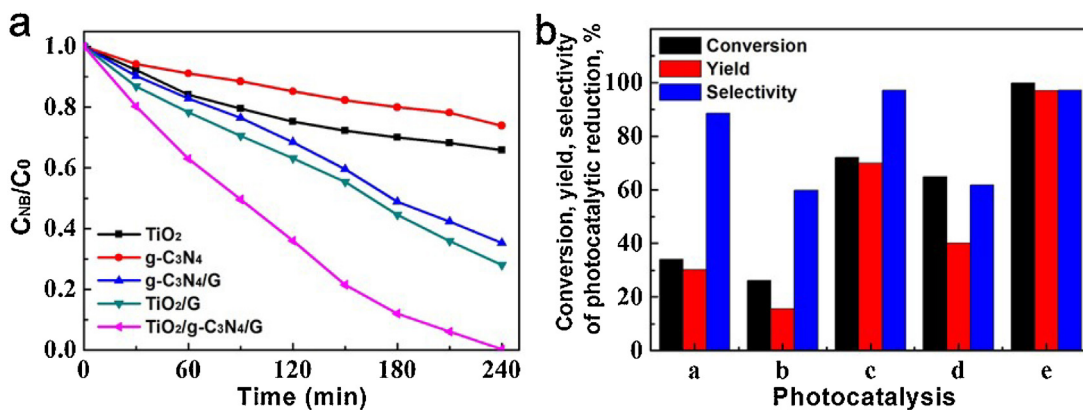


**Fig. 7.** (a) Photoreduction curves of the NB aqueous solutions containing different photocatalysts; (b) conversion, yield, selectivity of photocatalytic reduction (a:  $\text{TiO}_2$  NWs, b:  $\text{g-C}_3\text{N}_4$ , c:  $\text{TiO}_2/\text{G}$ , d:  $\text{g-C}_3\text{N}_4/\text{G}$ , e:  $\text{TiO}_2/\text{g-C}_3\text{N}_4/\text{G}$ ).

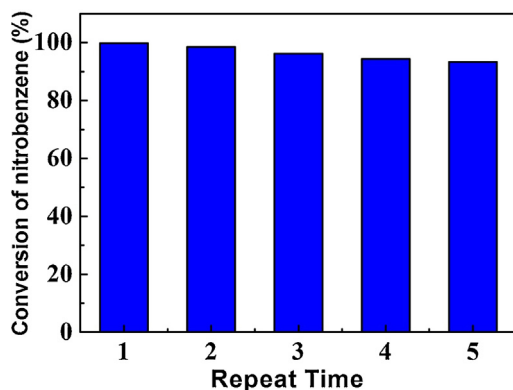


**Fig. 8.** Cycling runs in photo reduction of NB in the presence of TiO<sub>2</sub>/g-C<sub>3</sub>N<sub>4</sub>/G composite photocatalyst.

photocatalytic performance, including the conversion rate, yield and selectivity for the reduction of nitrobenzene are summarized in Fig. 7b. Restricted by the poor electronic conductivity together with the limited contact between graphene and g-C<sub>3</sub>N<sub>4</sub>, pure g-C<sub>3</sub>N<sub>4</sub> and g-C<sub>3</sub>N<sub>4</sub>/G both exhibit worse performance comparing with TiO<sub>2</sub> and TiO<sub>2</sub>/G, respectively. While the TiO<sub>2</sub>/g-C<sub>3</sub>N<sub>4</sub>/G displays the best performance, its conversion rate can reach 97%, and the yield and selectivity from nitrobenzene to aniline all exceed 97%. Additionally, it is found that TiO<sub>2</sub>/g-C<sub>3</sub>N<sub>4</sub>/G possesses a high stability (Fig. 8). Due to the unavoidable loss of catalysts during cycling tests, the photocatalytic activity of TiO<sub>2</sub>/g-C<sub>3</sub>N<sub>4</sub>/G only displays a little decrease (within 5%) after 5 cycles, indicating that the TiO<sub>2</sub>/g-C<sub>3</sub>N<sub>4</sub>/G remains active for long-term service without obvious deactivation.

### 3.7. Reaction mechanism

A possible mechanism for the selective reduction of nitrobenzene using TiO<sub>2</sub>/g-C<sub>3</sub>N<sub>4</sub>/G photocatalyst is illustrated in Fig. 9. Under visible light irradiation, both TiO<sub>2</sub> NWs and g-C<sub>3</sub>N<sub>4</sub> nanosheets absorb photons, which excite photo generated electrons to the conduction band (CB) and simultaneously produce photogenerated holes in the valence band (VB). With the presence of highly electronic conductive graphene which is well contacted with TiO<sub>2</sub> and C<sub>3</sub>N<sub>4</sub>, the electrons are readily transferred to the

graphene, thus forming an electron pool. In addition, the N<sub>2</sub> purge condition provides an anaerobic atmosphere for the reaction. Thus, the nitrobenzene has no opportunity to undergo the oxidation reaction. For the reduction of nitrobenzene, a photo-induced six-electron reduction process is involved [50]. At the same time, due to strong Van del walls interaction between graphene and nitrobenzene, nitrobenzene can be easily adsorbed on to the surface of graphene, and thus facilitating the reduction of nitrobenzene to aniline [51]. It is clear that the photo-generated holes and photo-generated electrons should play the same crucial roles in the oxidation-reduction coupling process. Evidently, complete reduction of 1 mol nitrobenzene should require six mol electrons. Meanwhile, the same numbers of holes (6 mol) are produced shown in Fig. S7. The photo-generated holes are quenched by methanol, which results in the methanol removing hydrogen atoms, and then oxidized to methanol [42,52].

## 4. Conclusion

A 3D heterostructure of TiO<sub>2</sub>/g-C<sub>3</sub>N<sub>4</sub>/G composite is fabricated via a simple self-assembly photochemical reduction method. The structure, surface morphology and element chemical states have been investigated. In this heterostructure, TiO<sub>2</sub> NWs not only act as a semiconductor to capture visible light, but also prevent graphene and g-C<sub>3</sub>N<sub>4</sub> nanosheets from restacking. Graphene nanosheets facilitate photo-induced electron transportation and separation, and g-C<sub>3</sub>N<sub>4</sub> broadens the spectral response and improves the light absorption in visual-region. Benefiting from the positive synergistic effect of the three components, 97% nitrobenzene can be converted into aniline within 4 h using TiO<sub>2</sub>/g-C<sub>3</sub>N<sub>4</sub>/G as the photocatalyst. Additionally, it is found that TiO<sub>2</sub>/g-C<sub>3</sub>N<sub>4</sub>/G possesses a high selectivity and stability during application. A possible photocatalytic mechanism is proposed based on the experimental results. Under visible light irradiation, both TiO<sub>2</sub> NWs and g-C<sub>3</sub>N<sub>4</sub> nanosheets absorbed photons, which excited plenty of photo generated electrons. Being a natural conductor, the graphene could greatly promote electron transfer from TiO<sub>2</sub> NWs and g-C<sub>3</sub>N<sub>4</sub> towards their surfaces, leading to the improvement of photocatalytic performance. Meanwhile, due to strong Van del walls interaction between graphene and nitrobenzene, nitrobenzene can be easily adsorbed on to the surface of graphene, facilitating the reduction of nitrobenzene to aniline.

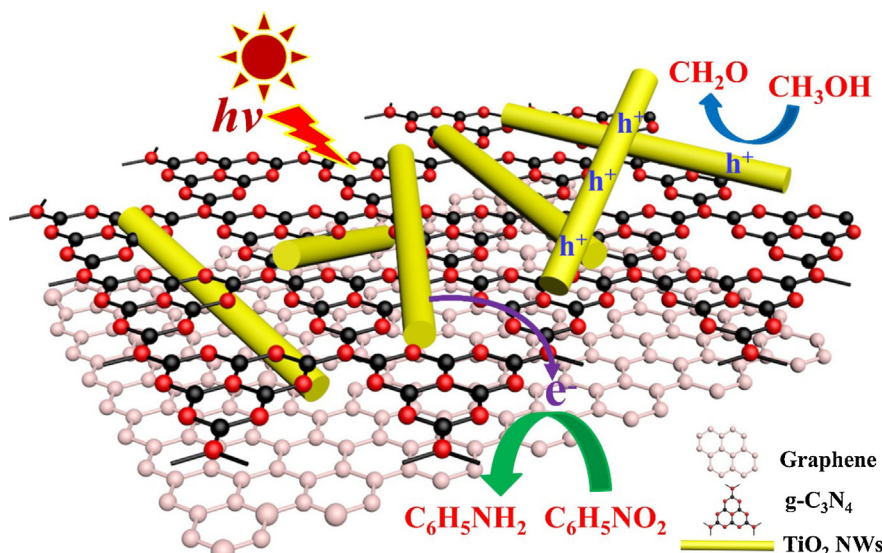


**Fig. 9.** Schematic diagram of photo-excited electrons and holes transfer among TiO<sub>2</sub> NWs, g-C<sub>3</sub>N<sub>4</sub> and graphene.

## Acknowledgments

This work was financially supported by the National Natural Science Foundation of China (Nos. 51401239, 21322609, 21576289, 51401157, 11404138), Shandong Provincial Natural Science Foundation of China (No. BS2014CL019), Key Program Project of National Natural Science Foundation of China (51231008), the National 973 program of China (2012CB619403), Thousand Talents Program of China, and Science Foundation of China University of Petroleum, Beijing (Nos. C201603, 2462015YQ0602).

## Appendix A. Supplementary data

Supplementary data associated with this article can be found, in the online version, at <http://dx.doi.org/10.1016/j.apcatb.2016.10.003>.

## References

- [1] J. Liu, Y. Liu, N. Liu, Y. Han, X. Zhang, H. Huang, Y. Lifshitz, S.-T. Lee, J. Zhong, Z. Kang, *Science* 347 (2015) 970–974.
- [2] X. Yang, J. Qin, Y. Jiang, K. Chen, X. Yan, D. Zhang, R. Li, H. Tang, *Appl. Catal. B: Environ.* 166/167 (2015) 231–240.
- [3] S.-i. Naya, T. Niwa, T. Kume, H. Tada, *Angew. Chem. Int. Ed.* 53 (2014) 7305–7309.
- [4] K. Imamura, T. Yoshikawa, K. Nakanishi, K. Hashimoto, H. Kominami, *Chem. Commun.* 49 (2013) 10911–10913.
- [5] K. Imamura, T. Yoshikawa, K. Hashimoto, H. Kominami, *Appl. Catal. B: Environ.* 134–135 (2013) 193–197.
- [6] P. Roy, A.P. Periasamy, C.-T. Liang, H.-T. Chang, *Environ. Sci. Technol.* 47 (2013) 6688–6695.
- [7] P.F. Vogt, J.J. Gerulis, *Ullmann's Encyclopedia of Industrial Chemistry*, Wiley-VCH Verlag GmbH & Co. KGaA, 2000.
- [8] J. Kaur, B. Pal, *Catal. Commun.* 53 (2014) 25–28.
- [9] A. Corma, P. Serna, *Science* 313 (2006) 332–334.
- [10] H. Zhu, X. Ke, X. Yang, S. Sarina, H. Liu, *Angew. Chem.* 122 (2010) 9851–9855.
- [11] F. Cárdenas-Lizana, S. Gómez-Quero, M.A. Keane, *Catal. Lett.* 127 (2009) 25–32.
- [12] T. Kamegawa, H. Seto, S. Matsuura, H. Yamashita, *ACS Appl. Mater. Interfaces* 4 (2012) 6635–6639.
- [13] S. Fuldnar, R. Mild, H.I. Siegmund, J.A. Schroeder, M. Gruber, B. Konig, *Green Chem.* 12 (2010) 400–406.
- [14] D. Cropek, P.A. Kemme, O.V. Makarova, L.X. Chen, T. Rajh, *J. Phys. Chem. C* 112 (2008) 8311–8318.
- [15] X. Chen, J. Wei, R. Hou, Y. Liang, Z. Xie, Y. Zhu, X. Zhang, H. Wang, *Appl. Catal. B: Environ.* 188 (2016) 342–350.
- [16] H. Zhang, X. Lv, Y. Li, Y. Wang, J. Li, *ACS Nano* 4 (2010) 380–386.
- [17] Y. Liang, H. Wang, H. Sanchez Casalongue, Z. Chen, H. Dai, *Nano Res.* 3 (2010) 701–705.
- [18] Y. Zhang, Z.-R. Tang, X. Fu, Y.-J. Xu, *ACS Nano* 4 (2010) 7303–7314.
- [19] J. Feng, Y. Hou, X. Wang, W. Quan, J. Zhang, Y. Wang, L. Li, *J. Alloys Compd.* 681 (2016) 157–166.
- [20] C. Liu, L. Zhang, R. Liu, Z. Gao, X. Yang, Z. Tu, F. Yang, Z. Ye, L. Cui, C. Xu, Y. Li, *J. Alloys Compd.* 656 (2016) 24–32.
- [21] S. Hoang, S. Guo, N.T. Hahn, A.J. Bard, C.B. Mullins, *Nano Lett.* 12 (2012) 26–32.
- [22] Y. Sang, Z. Zhao, J. Tian, P. Hao, H. Jiang, H. Liu, J.P. Claverie, *Small* 10 (2014) 3775–3782.
- [23] W. Zhou, Z. Yin, Y. Du, X. Huang, Z. Zeng, Z. Fan, H. Liu, J. Wang, H. Zhang, *Small* 9 (2013) 140–147.
- [24] N. Liu, V. Häublein, X. Zhou, U. Venkatesan, M. Hartmann, M. Mačković, T. Nakajima, E. Spiecker, A. Osvet, L. Frey, P. Schmuki, *Nano Lett.* 15 (2015) 6815–6820.
- [25] X. Pan, Y. Zhao, S. Liu, C.L. Korzeniewski, S. Wang, Z. Fan, *ACS Appl. Mater. Interfaces* 4 (2012) 3944–3950.
- [26] N. Wu, J. Wang, D.N. Tafen, H. Wang, J.-G. Zheng, J.P. Lewis, X. Liu, S.S. Leonard, A. Manivannan, *J. Am. Chem. Soc.* 132 (2010) 6679–6685.
- [27] S.D. Perera, R.G. Mariano, K. Vu, N. Nour, O. Seitz, Y. Chabal, K.J. Balkus, *ACS Catal.* 2 (2012) 949–956.
- [28] Q. Xiang, B. Cheng, J. Yu, *Appl. Catal. B: Environ.* 138–139 (2013) 299–303.
- [29] Y. Xue, X. Wang, *Int. J. Hydrogen Energy* 40 (2015) 5878–5888.
- [30] L. Chen, X. Zhou, B. Jin, J. Luo, X. Xu, L. Zhang, Y. Hong, *Int. J. Hydrogen Energy* 41 (2016) 7292–7300.
- [31] C. Zhang, Y. Zhu, *Chem. Mater.* 17 (2005) 3537–3545.
- [32] S. Yang, Y. Gong, J. Zhang, L. Zhan, L. Ma, Z. Fang, R. Vajtai, X. Wang, P.M. Ajayan, *Adv. Mater.* 25 (2013) 2452–2456.
- [33] Z. Tong, D. Yang, J. Shi, Y. Nan, Y. Sun, Z. Jiang, *ACS Appl. Mater. Interfaces* 7 (2015) 25693–25701.
- [34] R.C. Pawar, V. Khare, C.S. Lee, *Dalton Trans.* 43 (2014) 12514–12527.
- [35] S. Zhang, J. Li, X. Wang, Y. Huang, M. Zeng, J. Xu, *J. Mater. Chem. A* 3 (2015) 10119–10126.
- [36] Y. Zheng, Y. Jiao, L. Ge, M. Jaroniec, S.Z. Qiao, *Angew. Chem.* 125 (2013) 3192–3198.
- [37] S.M. Jung, H.Y. Jung, W. Fang, M.S. Dresselhaus, J. Kong, *Nano Lett.* 14 (2014) 1810–1817.
- [38] Y. Li, Z. Wang, X.-J. Lv, *J. Mater. Chem. A* 2 (2014) 15473–15479.
- [39] H. Li, Z. Xia, J. Chen, L. Lei, J. Xing, *Appl. Catal. B: Environ.* 168–169 (2015) 105–113.
- [40] J. Tian, Q. Liu, C. Ge, Z. Xing, A.M. Asiri, A.O. Al-Youbi, X. Sun, *Nanoscale* 5 (2013) 8921–8924.
- [41] V. Etacheri, J.E. Yourey, B.M. Bartlett, *ACS Nano* 8 (2014) 1491–1499.
- [42] X. Dai, M. Xie, S. Meng, X. Fu, S. Chen, *Appl. Catal. B: Environ.* 158–159 (2014) 382–390.
- [43] Y. Tang, D. Wu, S. Chen, F. Zhang, J. Jia, X. Feng, *Energy Environ. Sci.* 6 (2013) 2447–2451.
- [44] T.Y. Ma, Y. Tang, S. Dai, S.Z. Qiao, *Small* 10 (2014) 2382–2389.
- [45] Y. Wen, H. Ding, Y. Shan, *Nanoscale* 3 (2011) 4411–4417.
- [46] H. Feng, R. Cheng, X. Zhao, X. Duan, J. Li, *Nat. Commun.* 4 (2013) 1539.
- [47] G. Williams, B. Seger, P.V. Kamat, *ACS Nano* 2 (2008) 1487–1491.
- [48] Y. Zhang, Z.-R. Tang, X. Fu, Y.-J. Xu, *ACS Nano* 5 (2011) 7426–7435.
- [49] S. Thangavel, K. Krishnamoorthy, S.-J. Kim, G. Venugopal, *J. Alloys Compd.* 683 (2016) 456–462.
- [50] J.L. Ferry, W.H. Glaze, *Langmuir* 14 (1998) 3551–3555.
- [51] H. Wei, H. Jiang, Z. Zheng, Q. Zhao, Q. Wu, J. Zhan, *Mater. Res. Bull.* 48 (2013) 1352–1356.
- [52] R.M. Mohamed, E.S. Aazam, *J. Alloys Compd.* 595 (2014) 8–13.